J. Biochem. **139**, 71–80 (2006)
doi:10.1093/jb/mvj007

A Proteomic Assessment of Muscle Contractile Alterations during Unloading and Reloading

Younguk Seo[1], Kisoo Lee[1], Kyoungsook Park[2], Kiho Bae[1] and Inho Choi[1,*]

[1]Department of Life Science, College of Liberal Arts and Science, Yonsei University, Wonju, 220-710, Republic of Korea,; and [2]Molecular Therapy Research Center, Sungkyunkwan University, Seoul, 135-710, Republic of Korea

Received September 1, 2005; accepted September 28, 2005

Unloading of skeletal muscle causes atrophy and altered contractility. To identify major muscle proteins responding significantly to the altered loading and to elucidate how the contractile alterations reflect potential proteomic modifications, we examined protein expression in the rat soleus muscle during 3-week hindlimb suspension and 2-week reloading. Compared with unsuspended controls, experimental animals had a 0.5- to 0.6-fold decrease in tension during unloading and early reloading, comparable to 0.2- to 0.6-fold decreases in the protein levels of myosin light chain 1 (MLC1), α-actin, tropomyosin β-chain, and troponins T1 and T2. The observed 1.4- to 1.6-fold increase in shortening velocity appears to reflect 1.2- to 9.0-fold increases in the protein levels of fast-type MLC2, glycolytic enzymes, and creatine kinase, and 0.2- to 0.3-fold decreases in slow-type troponins T1 and T2. The levels of three heat shock proteins (p20, alpha crystallin B chain, and HSP90) decreased during unloading but returned to control levels during reloading. These results imply that proteomic responses to unloading change overall myofibrillar integrity and metabolic regulation, resulting in altered contractility.

Key words: antigravity, heat shock protein, metabolic enzyme, muscle contractility, myofibrillar protein.

Abbreviations: ANOVA, analysis of variance; 2-DE, 2-dimensional electrophoresis; F_o, maximal muscle force; HSP, heat shock protein; IPG, immobilized pH gradient; MLC, myosin light chain; R, reloading; U, unloading.

Mammalian antigravity muscles display remarkable morphological and functional adjustments to loading status (*1*). During unloading, the muscle loses significant mass and specific force but recovers normal levels during reloading (*2*, *3*). Muscle atrophy and functional depression during unloading are not merely the result of a proportional reduction in muscle volume or structural components (*e.g.*, proteins). Rather, this phenomenon occurs with disproportional changes in the levels of specific cellular components, and these changes may involve active regulation of gene expression and protein modifications (*4*, *5*). The disproportional changes in protein components result in tissue having different levels of actin versus myosin, aerobic *versus* anaerobic enzymes, and slow *versus* fast-type isoforms, thus leading to shifts in contractile capacity (*6–8*). For instance, unloading causes a preferential reduction in actin filaments over myosin filaments (*3*, *9*), and this change may result in the disruption of myofibrillar alignment and depression of muscle tension (specific force). In contrast, unloading causes an increase in fast-type myosin isoforms relative to slow-type isoforms, resulting in augmented shortening velocity (*3*).

Although general trends in the physiological responses of the tissue to unloading have been well established, it is still unclear as to what extent the biochemical components of the muscle change due to altered loading. Muscle contractility is determined by the integrated actions of myofibrillar and metabolic constituents (*1*). Thus, contractile shifts should be examined from the viewpoint of overall proteomic modifications of cellular components, rather than changes in the levels of individual components (*10*, *11*).

One may thus ask what specific kinds of proteins respond to unloading, and how well such modifications explain shifts in contractile functions. For example, previous studies found that, during unloading, the length and quantity of actin filaments are affected to a greater extent than are myosin filaments (*3*, *9*). To support this finding, we need to analyze the expression levels of mechanically sensitive contractile proteins as a whole, as changes in expression may cause significant modifications in myofilament conformation. Moreover, to understand the preferential upregulation of glycolytic metabolism over oxidative metabolism during unloading, we need to assess the levels of mechanically sensitive metabolic enzymes that would cause an increase in the shortening velocity of myofibers.

Regarding muscle responses to physical stress, it would also be interesting to observe whether an alteration in loading directly influences the expression of stress proteins, such as heat shock proteins (HSPs). Previous reports have revealed that several HSPs like HSP72 and α crystalline B are expressed in proportion to the number of slow oxidative fibers (relative to fast glycolytic fibers) in normal weight-bearing skeletal muscles (*12*, *13*). In the unloading condition, however, expression of HSPs may be downregulated to levels lower than those anticipated from the

*To whom correspondence should be addressed. Tel: +82-33-760-2244, Fax: +82-33-760-2183, E-mail: ichoi@dragon.yonsei.ac.kr

reduced number of slow fibers, implicating mechanical stress as a direct factor affecting HSP expression. If this were the case, changes in the levels of HSPs might additively affect modifications of the contractile and metabolic proteins during unloading. This reasoning arises from a number of previous reports showing that most HSPs act as molecular chaperones during protein folding, repairing, membrane translocation as well as general cytoprotection (*7*, *14–16*). Interestingly, elevated expression of HSPs (*e.g.*, HSP25, HSP72) in response to heat treatment significantly attenuates the atrophy of the unloaded or denervated rat soleus muscle (*17*, *18*). Thus, HSPs may be an important component of proteomic changes and myofiber protection in skeletal muscles during unloading and reloading.

Two-dimensional electrophoresis (2-DE) allows effective comparisons of protein expression patterns between normal and myopathic cells (*11*). According to Isfort *et al.* (*10*, *19*), the rat soleus muscle shows significant proteomic alterations during unloading (*i.e.*, denervation or hindlimb suspension) and reloading, and such alterations appear to proceed reciprocally. However, few reports have addressed the proteomic and contractile responses of the antigravity muscle during unloading and reloading within a single study.

Here we report the temporal profiling of protein expression in the rat soleus muscle during three weeks of unloading followed by two weeks of reloading. A hindlimb suspension model and 2-DE analysis were used to assess the effect of loading on muscle properties. Consistent with previous reports (*1*, *3*), we found that the soleus muscle showed decreased tension and increased shortening velocity during unloading, and these parameters returned to the control levels during reloading. The aims of the study were therefore to identify major muscle proteins responding significantly to the altered loading, and to elucidate how the potential proteomic modifications are reflected in the muscle contractile alterations.

MATERIALS AND METHODS

Animals—The study was approved by the Yonsei University Animal Care and Use Committee. Sprague-Dawley rats of four weeks of age (about 90 g) were reared at 22 ± 1°C in a 14:10 light:dark cycle. Standard Purina rat chow and water were provided ad libitum. On the last day of week four, the rats were randomly divided into seven groups: two unloading groups of 1 wk (U1w) and 3 wk (U3w); four reloading groups that experienced the 3-wk unloading followed by 1 h, 5 h, 1 d, or 2 wk of reloading (R1h, R5h, R1d, and R2w, respectively); and one representative age-matched control group kept for three weeks under standard conditions (C3w). In our preliminary studies, a 3-wk unloading period and 2-wk reloading period were sufficient to observe significant alterations in muscle mechanical properties (*20*),

Hindlimb Suspension—The hindlimb suspension model was described previously (*17*, *20*). Briefly, each animal was weighed and anesthetized intraperitoneally with pentobarbital sodium (30 mg kg^{-1}). Two pieces of flexible Tygon tubing (5.6 mm outside diameter) were placed along the dorsum of the animal and sutured with silk threads to provide a firm support. The animal was jacketed with a piece of nylon mesh that was sutured to the tubing for further support. The tail was taped gently to the Tygon tubing. On the following day (the first day of week five), after the animal had completely recovered from the anesthetic, the tubing at the tip of the tail was connected to a tether so that the animal was suspended tilting about 35° head-down. The animal was free to move around the cage on its front feet. We replaced the mesh jacket in about 10 days as the animal grew. We applied a similar tubing and jacket to the control groups, except that the tail was not taped to the tubing. At the time of reloading, the tubing and jacket were removed from the animals in both the unloading and control groups.

Muscle Preparation—Each animal was anesthetized with pentobarbital sodium (i.p., 50 mg kg^{-1}), and the soleus muscle tissues of both right and left hindlimbs were quickly removed. The left soleus muscle was frozen immediately in liquid nitrogen for 2-DE analysis. The right soleus muscle was soaked in 70 ml of cold oxygenated Ringer's solution (115 mM NaCl, 5 mM KCl, 4 mM $CaCl_2$, 1 mM $MgCl_2$, 1 mM NaH_2PO_4, 24 mM $NaHCO_3$, 11 mM glucose, pH 7.39) containing 0.02 g $liter^{-1}$ tubocurarine chloride. One tendon was tied to the 300B-LR servomotor arm (Aurora Scientific, Canada) and the other tendon to a micrometer to adjust to the optimal muscle length.

Muscle Contraction—The servo system has the ability to make both force and length steps in 1.3 ms and transition from length control to force control without any length transient. A custom software program (DMC, Aurora Scientific) was used to control both the servo system and a Grass S48 stimulator. The stimulator was connected to a pair of bright platinum electrodes and supplied a 1.0-ms square wave pulse or pulse train. Data on force or length changes were stored in a computer and analyzed by custom software (DMA, Aurora Scientific).

In all experiments ($n = 6$ for each group), tissue temperature was maintained at 25°C. For each preparation, we determined the optimal muscle length and supramaximal voltage that generated maximum twitch force. A stimulus frequency of 200 Hz was used to produce fully fused tetani for both the unloading-reloading groups and the control group. Maximum tetanic force (F_o) was stabilized, usually after the first three or four trials. A rest period of 20 min was given between electrical stimulations. Shortening velocity of the tissue was then examined at two values of loads where a near maximum power (= shortening velocity × load) was generated, as in a previous study (*20*). To find the two loads, we first measured shortening velocity of the muscle from quick-release isotonic contractions, with 10–12 preset loads ranging from 0.1–0.8 F_o. Length changes were measured over 10–50-ms periods starting about 10 ms after the release. A hyperbola was fitted to the data using Hill's equation, and force–velocity and power–velocity relationships were established (*1*). From these experiments (n = 4), we determined two loads, 0.35 F_o and 0.40 F_o, which best represented the forces generating near-maximal power (see "RESULTS"). We thus used these two load levels in the subsequent experiments to determine shortening velocities. We rechecked F_o after the shortening velocity measurement and discarded the muscle and data if this last F_o was less than 93% of the initially established F_o.

After each experiment, we measured the optimal muscle length in place using a micrometer under a light

microscope and approximated the muscle fiber length to be 2/3 the optimal muscle length (*20*). The tissue was frozen in place with liquid nitrogen, and its mass was measured with a chemical balance after tendons and connective tissues were removed. The muscle was then sectioned (8 μm) in a Microm HM505E cryostat and stained by a routine hematoxylin and eosin procedure. The cross-sectional area of the section was determined as in a previous study (*20*). Muscle force was normalized with cross-sectional area, and shortening velocity was normalized with fiber length.

Protein Extraction and Sample Preparation—The frozen soleus tissues for each group were crushed in liquid nitrogen using a mortar and pestle. The powdered sample was solubilized in 1 ml lysis buffer containing 7 M urea, 2 M thiourea, 65 mM DTT, 4% CHAPS, 40 mM Tris, 0.5% immobilized pH gradients (IPG) buffer (pH 3–10), and protein inhibitor Complete Mini (Roche, Penzberg, Germany). The sample then was incubated for 1 h at room temperature and centrifuged for 30 min at 12,000 × *g* at 4°C. The supernatant was collected, and its protein concentration was determined using a Bradford assay kit (Bio-Rad, Hercules, CA, USA), as in a previous study (*21*). For each tissue, a protein sample of 1.2 mg was used for 2-DE.

Separation of Proteins by 2-DE—Solubilized protein was incubated at 30°C for 30 min with endonuclease (Sigma Chemical, St. Louis, USA) and centrifuged for 15 min at 12,000 × *g* at 4°C. The final sample proteins were mixed with a rehydration buffer [7 M urea, 2 M thiourea, 65 mM DTT, 4% CHAPS, 40 mM Tris, 0.5% IPG buffer (pH 3–10)] to obtain a total volume of 450 μl. The first dimension isoelectric separation of the sample proteins was made on IPG of 3–10 liters (240 × 3 × 0.5 mm) dry strips (Amersham Pharmacia Biotech, Little Chalfont, Bucks, UK) using an Ettan IPGphor Isoelectric Focusing System (Amersham Pharmacia Biotech). The strips were rehydrated at 60 V for 12 h, and focusing was run for 91,420 Vh using a gradually increasing voltage protocol implemented by a programmable high-voltage power supply (final voltage 8,000 V). Following isoelectric focusing, the strips were equilibrated for 15 min in 10 ml tributyl phosphine (TBP) solution [6 M urea, 2% SDS, 50 mM Tris-HCl gel buffer, 30% (v/v) glycerol (87% v/v), 5 mM TBP].

The second dimensional separation was conducted with an Ettan DALT/six Electrophoresis Unit (Amersham Pharmacia Biotech) on 12% SDS polyacrylamide gels. The strips were embedded in 0.5% agarose stacking gel, and the proteins were separated for 12 h at 30 mA per gel until the bromophenol blue marker dye ran off the bottom of the gel.

After 2-DE, gels were fixed for 12 h in a mixture of 45% methanol and 5% phosphoric acid; they were then stained for 6 h in a solution of 0.1% Coomassie Brilliant Blue G-250, 17% ammonium sulfate, 3.6% phosphoric acid, and 34% methanol. The gels were then destained for 2 h by diffusion in a mixture of 15% methanol and 1% acetic acid, followed by washing for 1 h in deionized distilled water.

Quantitative Analysis—Stained gels were scanned using a PowerLook 1100 scanner (UMAX Technology, Dallas, Texas). The scanned images were processed with ImageMaster Analysis software (Amersham Pharmacia Biotech) to yield a list of position (pI/molecular weight) and volume information for each detected spot. Quantification of spot volumes was attempted in two ways: (i) Spot volumes were normalized by expressing the raw volume of each individual spot on a gel as a percentage of the total volume of protein present on that gel; and (ii) Spot volume was calculated by subtracting the background, thus yielding the raw spot volume minus the background intensity of the gel. We used the first approach because it offered better reproducibility since normalization standardized differences in the total amount of proteins present on each gel.

Protein Identification—Among more than 550 detectable protein spots on the gels, we screened 100–105 candidate spots having relatively accurate spot volume measurements from the scanned gel images. We then chose 34 spots based on statistically significant differences in the volumes across the unloading–reloading periods (see below in "Data Analysis"). These spots were excised from the Coomassie-stained gels. Excised spots were destained, reduced, alkylated, and then digested with trypsin (Promega, Madison, WI, USA) as previously described (*22*). Tryptic peptides were desalted and purified as described previously (*22*). Recovered peptides were prepared for MALDI-TOF MS by mixing with alpha-cyano-4-hydroxycinnamic acid and 1% formic acid in 50% acetonitrile, and droplets were allowed to dry on the MALDI sample plate. Peptide mass fingerprinting was performed using a Voyager DE-PRO MALDI-TOF MS (Applied Biosystems, Foster City, CA, USA), equipped with a 337-nm nitrogen UV laser. The instrument was operated at accelerating voltage of 20 kV in the reflection/delayed extraction mode, grid voltage of 76%, guide wire voltage of 0.02%, and a delay time of 150 ns. Proteins were identified from the peptide mass maps using MS-FIT (http://prospector.ucsf.edu), MASCOT (http://www.matrixscience.com/search_form_select.html), and ProFound (http://129.85.19.192/profound_bin/WebProFound.exe) to search the protein databases, SWISS-PROT (Version 44.1) and GenBank. All the searches were analyzed using a 50-ppm mass tolerance.

Data Analysis—All data are presented as mean ± 1 SE, unless otherwise noted. To find major proteins for which expression was significantly affected by the loading status, we examined differences in means of protein expression levels among groups using one-way analysis of variance (ANOVA) and Duncan's *post hoc* multiple comparison tests. Because differentiation of the soleus muscle is complete before postnatal week four (*23*) and the contractile properties of the muscle are statistically indistinguishable among animals at ± 2 weeks of age (*20*), we assumed that the C3w control animals were suitable for all experimental groups. Statistical procedures were performed using SPSS/PC+ (SPSS Inc.)

RESULTS

Muscle Atrophy—The soleus muscle of the subjects underwent significant atrophy during three weeks of unloading and until one day of reloading (R1d) (Fig. 1A). Muscle mass relative to body mass decreased 0.59-fold in U3w, and recovered to the control level in R2w (one-way ANOVA and Duncan's test, $F_{6,41} = 6.54$, $P < 0.001$).

Muscle Tension and Shortening Velocity—Maximum tetanic tension and shortening velocity of the soleus muscle

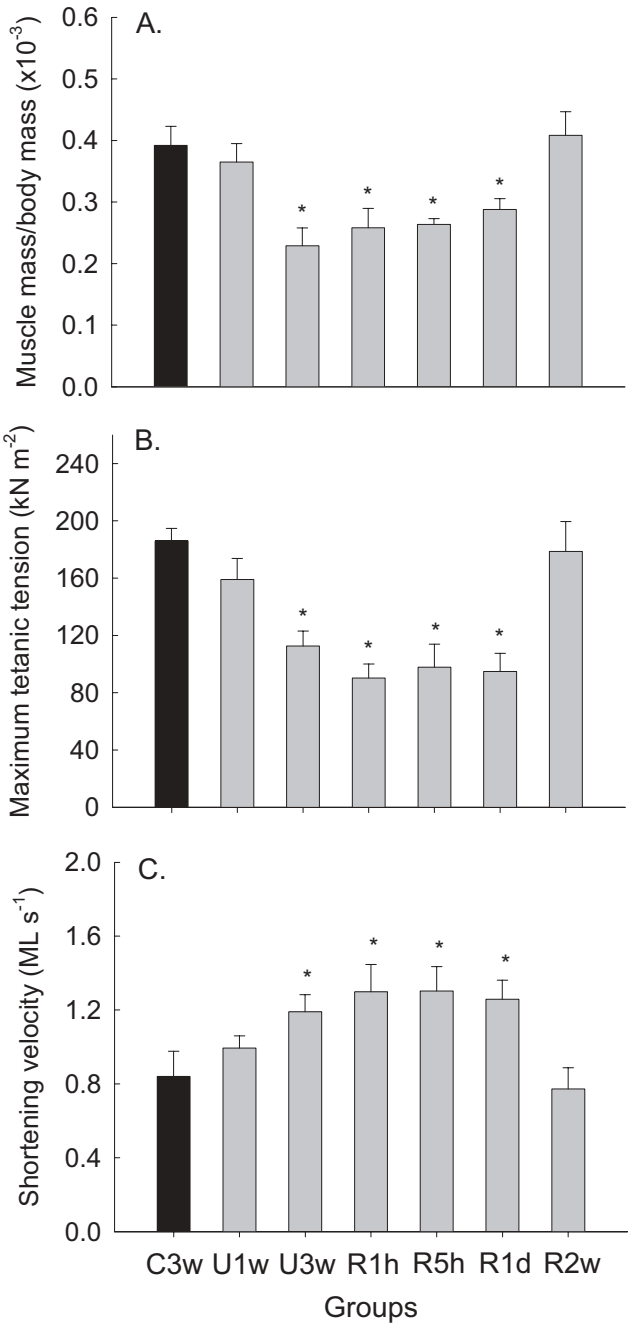

Fig. 1. **Effects of loading conditions on the soleus muscle mass relative to body mass (A), maximum tetanic tension (B), and shortening velocity (C).** The tension and shortening velocity were generated at 25°C by a 1.0-ms pulse at supramaximal voltage and a stimulation frequency of 200 Hz. Each data point represents the mean ± 1 SE (n = 6). *A significant difference from C3w (one-way ANOVA and Duncan's *post hoc* test, $P < 0.05$).

showed opposite trends during unloading and reloading (Fig. 1, B and C). The tetanic tension was 185.9 kN m^{-2} in the control, decreased 0.48- to 0.61-fold during U3w–R1d, and returned to the control level at R2w ($P < 0.001$). There was no significant difference in tension among U3w, R1h, R5h, and R1d (Duncan's test, $P > 0.05$). The shortening velocity was 0.84 ML s^{-2} in the control, increased 1.42- to 1.55-fold during U3w–R1d ($P < 0.01$), and returned to the control level at R2w (Fig. 1C). The velocity among the U3w, R1h, R5h, and R1d groups did not differ significantly.

Proteomic Responses to the Loading Condition—We found that 34 spots showed different levels of expression depending on the loading conditions (one-way ANOVA and Duncan's test, $P < 0.05$). Among these, MALDI-TOF analysis identified 27 proteins that were associated with contractile, metabolic, and stress responses of muscle. Protein identification of the corresponding spot numbers is summarized in Table 1. Figure 2, A–D, shows four typical proteome maps from C3w, U3w, R5h, and R2w. Figure 3 illustrates comparisons of spot volume for eight representative proteins among control, unloaded, and reloaded tissues. From these analyses, the change in volume of each spot is presented as a value relative to the control in Tables 2–5. The results are presented below.

Contractile Proteins (Table 2)—The levels of tropomyosin β-chain, α-actin, and myosin essential light chain (MLC1) decreased 0.64- to 0.66-fold during U3w to R1h and returned to the control level after two weeks of reloading. Myosin regulatory light chain (MLC2) was identified as three isoforms. The cardiac isoform decreased 0.3-fold in U3w and returned to the control level at R2w, whereas the two skeletal isoforms showed 3.0- to 6.0-fold increases at U3w and returned to the control level at R2w. Levels of both troponin T1 and T2 (parts of the troponin complex) showed 0.2- to 0.4-fold decreases in U3w and 1.3- to 1.4-fold increases at R2w.

Metabolic Proteins (Table 3)—We identified four enzymes associated with anaerobic metabolism that showed significant alteration in expression upon the varying loads. The level of glycogen phosphorylase, which catalyzes the breakdown of glycogen to glucose, increased 1.2- to 2.0-fold during the 3-wk unloading and the first 5 h of reloading, after which it returned to the control level at R2w. The level of fructose-bisphosphate aldolase A, which catalyzes the hydrolysis of fructose-1,6-bisphosphate into glyceraldehyde 3-phosphate and dihydroxyacetone phosphate, increased 9-fold at U3w and R1h and then rapidly returned to the control level after 5 h reloading. The level of beta enolase, an enzyme catalyzing the conversion of 2-phosphoglycerate to phosphoenolpyruvate, increased 4- to 6-fold during the 3-wk unloading to R1d and then returned to the control level at R2w. The lactate dehydrogenase B level changed only slightly during unloading and early reloading, but increased 1.8-fold at R2w.

Four aerobic enzymes showed significant changes upon varied loading: pyruvate dehydrogenase, aconitate hydratase (aconitase), malate dehydrogenase, and ATP synthase beta chain mitochondrial precursor. Pyruvate dehydrogenase, which catalyzes the conversion of pyruvate to acetyl CoA in the first step of the citric acid cycle, showed little change in expression level in U3w, but the level increased 1.6-fold at R1d. The level of aconitase, which catalyzes the hydration of cis-aconitate in the citric acid cycle, increased 1.9 and 2.2-fold during U3w–R1h and then returned to the control level after R5h. The level of malate dehydrogenase, which functions in the citric acid cycle, fatty acid synthesis, gluconeogenesis, and the malate-aspartate shuttle (*24*), increased about 1.5- to 1.8-fold during U1w–R5h and then returned to its control level

Table 1. **Summary of 27 identifiable proteins that showed significant differences in expression levels among the seven groups.**

Spot No.	Accession number	Protein identification	DB score	Coverage (%)	Peptides matched	Major decision DB	Estimated pI/Mw	
							pI	Mw
1	gi|346655	tropomyosin β-chain, skeletal muscle	53	15	7	MASCOT	4.64	32.781
2	gi|4501881	α-actin	83	29	8	MASCOT	5.23	42.024
4	P16409	myosin essential light chain (MLC1), skeletal isoform	4.932e+06	60	10	MS-FIT	5.08	20.64
7	P08733	myosin regulatory light chain (MLC2), cardiac isoform	4.773e+05	46	9	MS-FIT	4.93	17.769
8	P97457	myosin regulatory light chain (MLC2), skeletal isoform	1.039e+04	18	5	MS-FIT	4.83	17.056
9	P97457	myosin regulatory light chain (MLC2), skeletal isoform	4.682e+05	40	9	MS-FIT	4.89	17.056
11	gi|33465562	troponin T1, slow skeletal muscle	107	44	9	MASCOT	5.90	31.874
12	P16125	lactate dehydrogenase B-chain	1.018e+07	28	9	MS-FIT	5.75	31.979
13	gi|33465564	troponin T2, slow skeletal muscle	139	44	11	MASCOT	6.03	31.323
14	P14152	malate dehydrogenase	9.225e+04	20	7	MS-FIT	6.19	30.758
17	P97541	heat shock 20 kDa like protein, p20	7.405e+04	43	6	MS-FIT	6.25	17.679
18	P02770	serum albumin precursor	9.301e+06	27	12	MS-FIT	5.92	72.860
19	P02770	serum albumin precursor	4.171e+05	21	9	MS-FIT	6.10	70.698
20	P15429	beta enolase	5.727e+07	27	11	MS-FIT	8.05	45.611
22	P23927	alpha crystallin B chain	3.651e+04	34	5	MS-FIT	8.11	18.608
23	gi|40538860	aconitate hydratase mitochondrial precursor	187	28	19	MASCOT	8.36	85.539
24	P09812	glycogen phosphorylase muscle form	2.789e+08	23	14	MS-FIT	8.29	86.248
25	P00564	creatine kinase M chain	4.771e+10	51	19	MS-FIT	7.80	38.59
27	gi|1374715	ATP synthase β-chain mitochondrial precursor	94	32	9	MASCOT	5.02	49.357
29	P34058	heat shock protein 90 kDa	7.559e+10	31	17	MS-FIT	5.03	89.599
33	P49432	pyruvate dehydrogenase	2.594e+07	32	9	MS-FIT	5.41	30.053
37	P01946	hemoglobin α-1 and α-2 chains	2874	43	4	MS-FIT	8.81	19.414
41	P09605	creatine kinase mitochondrial precursor	6.719e+10	34	16	MS-FIT	8.86	37.232
42	P05065	fructose bisphosphate aldolase A	1691	36	8	MS-FIT	9.04	37.141
44	P12346	serotransferrin precursor (β1 metal binding globulin)	3.048e+07	18	10	MS-FIT	7.44	83.729
46	P12346	serotransferrin precursor (β1 metal binding globulin)	5.109e+09	20	13	MS-FIT	6.79	85.398
49	P14141	carbonic anhydrase III	4.644e+05	20	13	MS-FIT	8.30	23.034

by R2w. The ATP synthase beta chain, which is part of the H^+ transporting channel in the inner mitochondrial membrane that facilitates ATP synthesis, showed a 1.2-fold increase at U1w and R1h and then returned to the control level after R5h.

Stress Proteins (Table 4)—We identified three HSPs that showed considerable changes in expression during unloading and reloading. The levels of two small heat shock proteins, heat shock 20-kDa-like protein (p20) and alpha crystallin B chain, which are believed to function in the organization and maintenance of myofibrils (*16*, *25*), decreased 0.2- to 0.3-fold in U3w and R1h–R5h but recovered to control levels at R2w. The level of the 90-kDa heat shock protein (HSP90), which stabilizes proteins before folding or activation (*26*), also decreased 0.3- to 0.4-fold during U3w–R5h, after which it returned to the control level at R2w.

Regulatory and Plasma Proteins (Table 5)—We found at least three enzymes associated with metabolic regulation that changed significantly upon altered loading. The levels of creatine kinase M chain and creatine kinase ubiquitous mitochondrial precursor, which reversibly catalyze the transfer of phosphate between ATP and creatine phosphate (CrP) (*24*), increased 1.8- to 4.0-fold in U3w and then returned to control levels at R2w. The level of carbonic anhydrase III, which catalyzes the reversible hydration of CO_2 and HCO_3, decreased 0.7-fold during U3w–R1h and then gradually returned to the control level by R2w.

Among the plasma proteins identified, serum albumin precursor increased 1.5- to 2.2-fold during U3w–R5h and then returned to the control level at R2w. Serum albumin plays a role in maintaining the osmotic pressure of blood, transporting cations and hormones, and carrying free fatty acids from adipocytes to cells having metabolic needs (*24*). Hemoglobin alpha-1 and alpha-2 chain also increased 1.6- to 1.8-fold in U3w and R1h. The relative levels of serotransferrin precursor, which transports iron from the intestine and damaged erythrocytes to cells, increased 2.2- to 3.9-fold during U3w–R5h and returned to the control level at R2w.

DISCUSSION

Our data show that the extent of soleus muscle atrophy (Fig. 1A) was similar to that seen in previous studies (*7*). Muscle atrophy is induced primarily as a consequence of imbalanced maintenance of protein levels in the unloaded cell, which results from a decrease in protein synthesis and an increase in protein degradation (*27*, *28*), which are the consequence of transcriptional regulation (*29*, *30*). Because discordant changes in protein regulation can cause contractile and locomotor problems, finding countermeasures against these problems has been a central issue in space medicine and rehabilitation. Our original aim was to explore how such contractile changes reflect the biochemical imbalance during unloading and reloading.

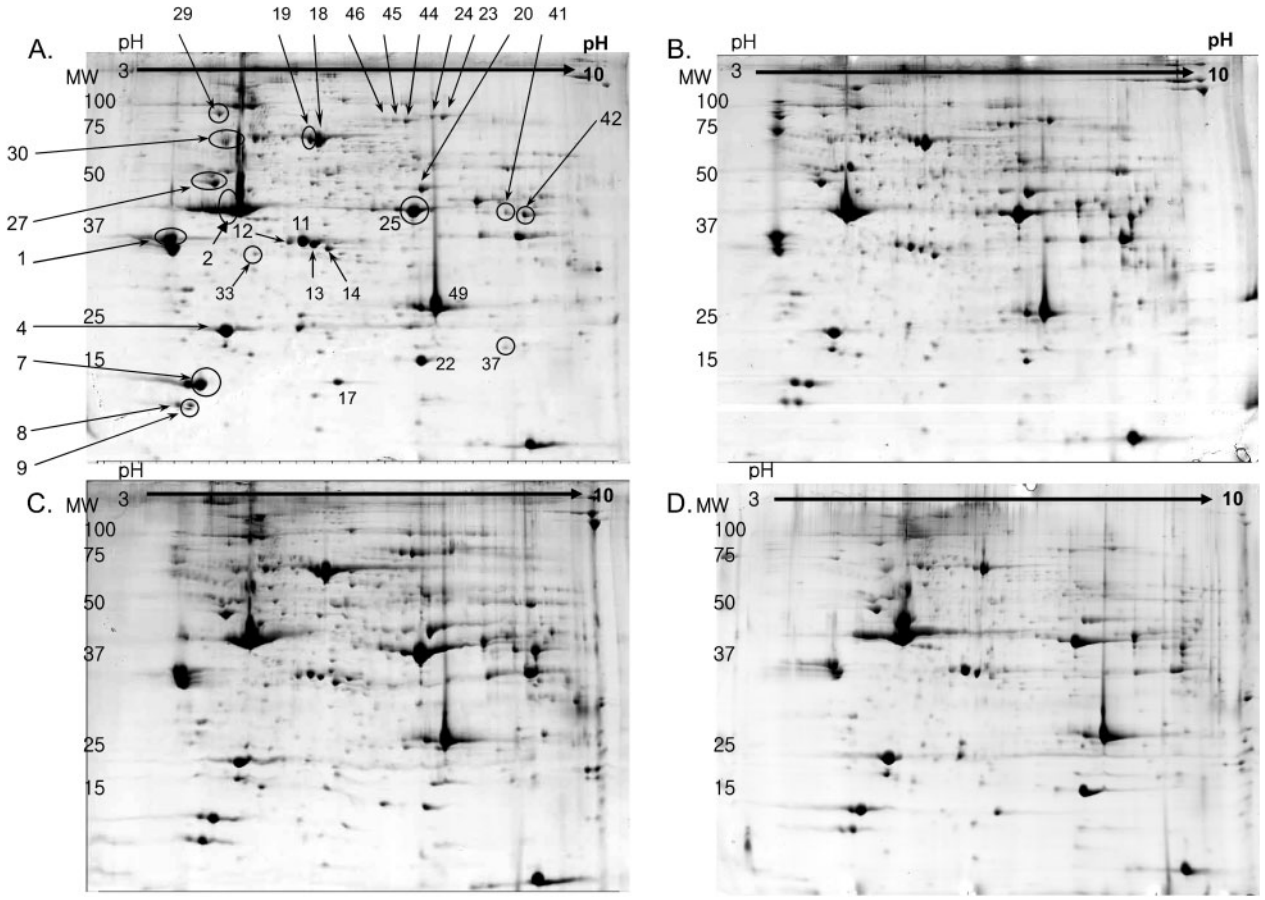

Fig. 2. **Representative 2-DE gel maps of the soleus muscle for C3w (A), U3w (B), R5h (C), and R2w (D).** Protein samples (1.2 mg) extracted from the soleus tissue were separated on a wide-range (pH 3–10) IPG L strip in the first dimension followed by a 12% SDS–polyacrylamide gel in the second dimension. The gel was stained with Coomassie blue. Numbered spots indicate a statistically significant change in relative expression level during unloading and reloading (the corresponding proteins are listed in Table 1).

Muscle Tension—The 0.5- to 0.6-fold decrease in tension during unloading and early reloading was comparable to 0.2- to 0.6-fold decreases in the levels of MLC1, α-actin, tropomyosin β-chain, and troponin T1 and T2. Muscle tension is determined by the interaction of myofilament proteins, and so if a part of the system were changed then tension development would be affected. Our data suggest that downregulation of the contractile proteins may result in conformational changes in myofilaments. Fibrous actin is a highly dynamic structure that is continually gaining and losing α-monomers (*24*, *31*). Unloading may enhance breakdown and/or reduce synthesis of these monomers after they dissociate from filament polymers. Furthermore, integrity of the actin filament could be disrupted during unloading, since alignment of fibrous actin with tropomyosin and troponin T might be seriously disturbed due to the disproportional reduction in their levels. In addition, the MLC1 level could be another factor causing tension depression during unloading. The decreased level of this protein may cause myosin heavy chains to be structurally less stable and enzymatically less active during cross-bridge formation (*32*). As the levels of both aerobic and anaerobic enzymes were elevated during unloading and early reloading (Table 3; also see below), the energy supply is unlikely to be the limiting factor in force development during the period.

Shortening Velocity—The 1.4- to 1.6-fold increase in shortening velocity during the unloading and reloading period appears to reflect the 3- to 6-fold increase in the fast-type MLC2, the 1.2- to 9-fold increase in glycolytic enzymes and the 1.8- to 4-fold increase in creatine kinase muscle chain and mitochondrial precursor, together with the 0.2- to 0.3-fold decrease in slow-type troponin T1 and T2 (Tables 2, 3 and 5). These results indicate that the transformation of the unloaded tissue toward fast-type features is characterized by upregulated fast-type MLC2, and elevation of glycolytic and phosphagen-supply capacity, and of shortening velocity. These features are important for determining turnover rates of cross-bridge formation and thus shortening velocity. The extent of the increase in shortening velocity might be limited by those proteins (*e.g.*, glycogen phosphorylase) that showed the smallest increases in their expression levels. The cellular response to unloading may occur in the metabolic enzymes first, followed by structural proteins, as suggested by Cros *et al*. (*33*). According to these authors, transcription of muscle creatine kinase and a glycolytic enzyme

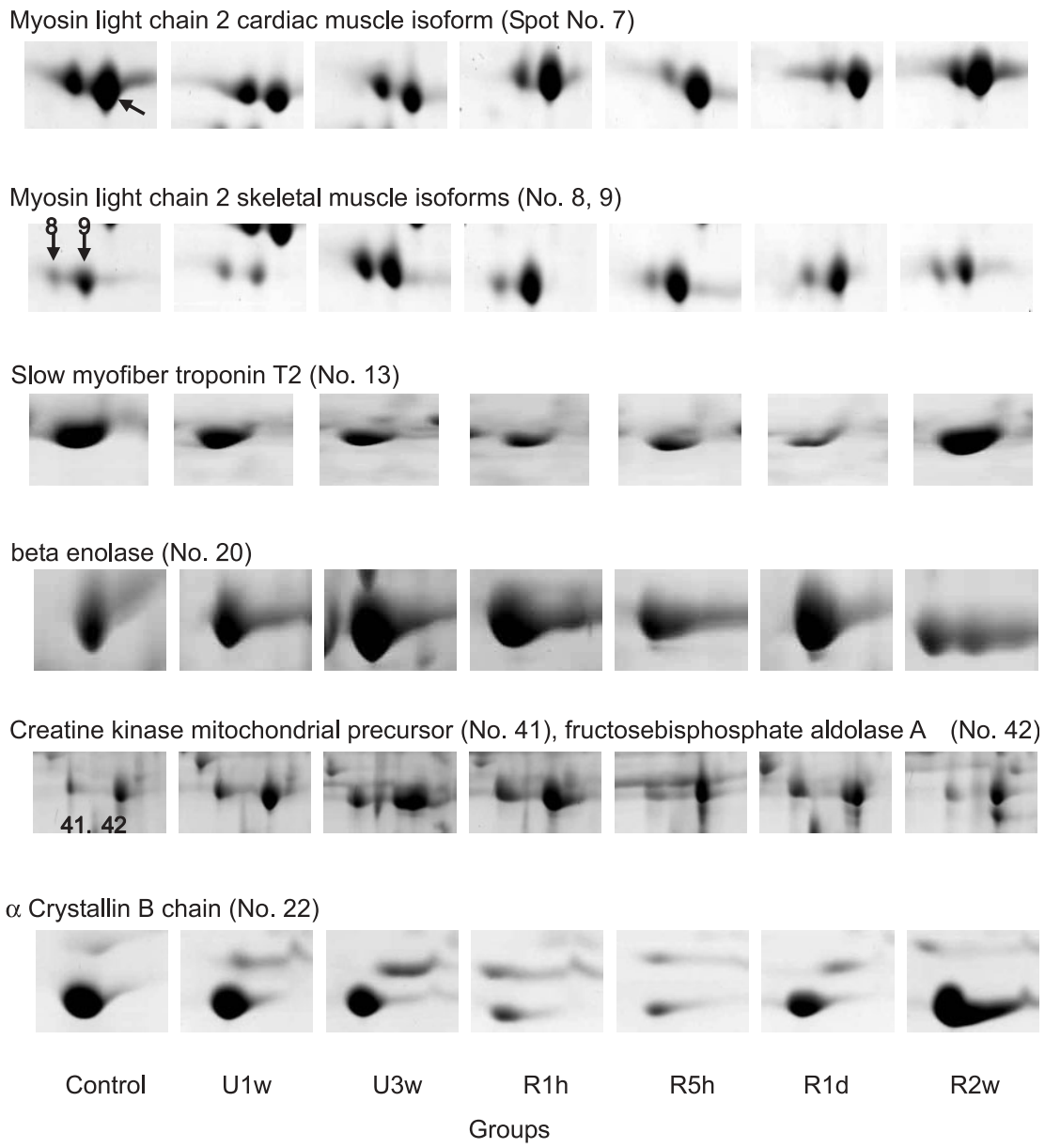

Fig. 3. **Comparisons of spot volumes across the loading status for eight representative proteins.** The proteins shown in the series of images in each panel were obtained from muscles from the same subjects.

(glyceraldehyde-3-phosphate dehydrogenase) preceded that of fast-isoform myosin heavy chains.

Stress Proteins—Expression levels of three HSPs, p20, alpha crystallin B chain, and HSP90, were 0.2- to 0.4-fold that of the control during unloading and early reloading (Table 4). These levels were much lower than that of the slow fibers (0.6- to 0.8-fold of the control) in the soleus muscle during 2–3 weeks of unloading (*7*), suggesting that HSP expression seemed to be directly affected by the altered mechanical stress. A similar decrease in the expression of these proteins has been reported in denervated or hindlimb-suspended soleus muscle (*10*, *19*, *25*, *34*). Other than their ubiquitous functional properties (*35*), cellular regulation of these proteins seems crucial to organization, protection and maintenance of myofibrillar structure. The two small HSPs (p20, α-crystallin B chain) are localized in specific sarcomeric structures, such as Z- or I-bands, that interact with actins and intermediate filaments, and are suggested to protect or maintain myofibrils and cytoskeletal structures against severe mechanical stresses (*14–16*). These two proteins, together with HSP27, also form co-oligomers that are unique to muscle cells (*16*). HSP90 acts as a molecular chaperone in the initial folding and assembly of myosin filaments in striated muscle (*26*). In addition, this protein has been reported to be a co-chaperone of the myosin assembly protein, UNC-45, during myogenesis (*36*). Taken together, the three HSPs were sensitive in their response to mechanical stress, and have a potential role in linking myofibrillar integrity with muscle contractile function.

Table 2. **Effects of loading on expression levels of eight contractile proteins. The levels are presented as values relative to C3w for that protein (n = 5).**

Names of proteins	Relative to C3w (fold ± 1SE)						
	C3w	U1w	U3w	R1h	R5h	R1d	R2w
Tropomyosin β-chain, skeletal isoform	1.0	0.91 ± 0.09	0.66 ± 0.12*	0.68 ± 0.14	1.03 ± 0.10	0.99 ± 0.14	0.89 ± 0.08
α-actin	1.0	0.75 ± 0.09*	0.74 ± 0.04*	0.66 ± 0.04*	0.89 ± 0.14	0.83 ± 0.18	1.10 ± 0.10
MLC1, skeletal muscle isoform	1.0	0.86 ± 0.05	0.67 ± 0.05*	0.64 ± 0.06*	0.68 ± 0.06*	0.70 ± 0.09*	0.87 ± 0.16
MLC2, cardiac muscle isoform	1.0	0.56 ± 0.05*	0.32 ± 0.07*	0.56 ± 0.13*	0.66 ± 0.06*	0.67 ± 0.12*	1.15 ± 0.08
MLC2, skeletal muscle isoform	1.0	2.87 ± 1.05*	6.07 ± 2.62*	4.15 ± 1.58*	2.14 ± 0.71	3.32 ± 0.69*	1.35 ± 0.53
MLC2, skeletal muscle isoform	1.0	1.27 ± 1.07	2.86 ± 0.81*	2.88 ± 0.07*	2.86 ± 1.06*	6.51 ± 4.98	0.84 ± 0.33
Troponin T1, slow skeletal muscle	1.0	0.63 ± 0.13*	0.38 ± 0.10*	0.40 ± 0.10*	0.27 ± 0.06*	0.58 ± 0.34	1.27 ± 0.23
Troponin T2, slow skeletal muscle	1.0	0.68 ± 0.21	0.34 ± 0.08*	0.41 ± 0.08*	0.20 ± 0.07*	0.75 ± 0.34	1.40 ± 0.29

*Significant differences among groups for that protein (one-way ANOVA and Duncan's *post hoc* multiple comparison tests, $P < 0.05$).

Table 3. **Effects of loading on expression levels of eight metabolic enzymes. The levels are presented as values relative to C3w for that protein (n = 5).**

Names of proteins	Relative to C3w (fold ± 1SE)						
	C3w	U1w	U3w	R1h	R5h	R1d	R2w
Glycogen phosphorylase	1.0	1.22 ± 0.06*	1.21 ± 1.84	1.84 ± 0.55*	0.60 ± 0.19	2.02 ± 0.92	1.03 ± 0.09
Fructose bisphosphate aldolase A	1.0	4.54 ± 2.26*	9.06 ± 3.76*	9.13 ± 4.33*	2.61 ± 1.28	1.40 ± 0.45	0.88 ± 0.41
Beta enolase	1.0	4.01 ± 1.06*	6.21 ± 0.44*	4.96 ± 3.09	5.48 ± 0.47*	5.28 ± 0.79*	2.35 ± 0.21*
Lactate dehydrogenase B-chain	1.0	0.99 ± 0.11	0.76 ± 0.12	0.84 ± 0.25	1.23 ± 0.46	1.42 ± 0.42	1.77 ± 0.37*
Pyruvate dehydrogenase	1.0	1.31 ± 0.30	1.18 ± 0.19	1.45 ± 0.37	1.39 ± 0.15*	1.64 ± 0.36*	0.81 ± 0.09
Aconitate hydratase mitochondrial precursor	1.0	1.53 ± 0.31	1.87 ± 0.22*	2.15 ± 0.30*	1.20 ± 0.14	1.39 ± 0.19	1.13 ± 0.15
Malate dehydrogenase	1.0	1.83 ± 0.33*	1.49 ± 0.09*	1.57 ± 0.06*	0.79 ± 0.08	1.06 ± 0.07	0.87 ± 0.11
ATP synthase β-chain mitochondrial precursor	1.0	1.22 ± 0.11*	1.03 ± 0.07	1.22 ± 0.08*	0.96 ± 0.10	0.78 ± 0.09	0.75 ± 0.12

*Significant differences among groups for that protein (one-way ANOVA and Duncan's *post hoc* multiple comparison tests, $P < 0.05$).

Table 4. **Effects of loading on three stress protein levels, presented as relative values to C3w for that protein (n = 5).**

Names of proteins	Relative to C3w (fold ± 1SE)						
	C3w	U1w	U3w	R1h	R5h	R1d	R2w
Heat shock 20 kDa like protein, p20	1.0	0.69 ± 0.21	0.31 ± 0.07*	0.30 ± 0.12*	0.16 ± 0.05*	0.50 ± 0.17*	1.27 ± 0.26
α-crystallin B chain	1.0	0.79 ± 0.11	0.34 ± 0.06*	0.15 ± 0.06*	0.18 ± 0.07*	0.59 ± 0.11*	1.07 ± 0.19
Heat shock protein 90 kDa	1.0	0.64 ± 0.19	0.39 ± 0.03*	0.34 ± 0.15*	0.41 ± 0.27*	0.64 ± 0.13*	1.21 ± 0.20

*Significant differences among groups for that protein (one-way ANOVA and Duncan's *post hoc* multiple comparison tests, $P < 0.05$).

Table 5. **Effects of loading on the levels of sarcoplasmic or plasma proteins, presented as relative values to C3w (n = 5).**

Names of proteins	Relative to C3w (fold ± 1SE)						
	C3w	U1w	U3w	R1h	R5h	R1d	R2w
Creatine kinase M-chain	1.0	1.53 ± 0.02*	1.82 ± 0.26*	1.54 ± 0.18*	1.55 ± 0.14*	1.34 ± 0.23	0.92 ± 0.07
Creatine kinase mitochondrial precursor	1.0	2.16 ± 0.94	3.95 ± 0.78*	4.33 ± 1.08*	1.37 ± 0.31	1.56 ± 0.51	0.69 ± 0.15
Carbonic anhydrase III	1.0	0.95 ± 0.06	0.75 ± 0.07*	0.72 ± 0.07*	0.83 ± 0.12	0.82 ± 0.13	1.06 ± 0.12
Serum albumin precursor	1.0	0.95 ± 0.38	1.55 ± 0.36*	2.06 ± 0.44*	1.36 ± 0.11*	1.32 ± 0.21*	0.91 ± 0.35
Serum albumin precursor	1.0	0.96 ± 0.16	1.47 ± 0.18*	2.00 ± 0.27*	2.24 ± 0.27*	1.71 ± 0.44*	1.15 ± 0.39
Hemoglobin α-1 and α-2 chain	1.0	1.24 ± 0.28	1.63 ± 0.25*	1.82 ± 0.21*	1.30 ± 0.45	1.42 ± 0.58	0.88 ± 0.32
Serotransferrin precursor	1.0	1.05 ± 0.17	2.60 ± 0.51*	2.97 ± 0.60*	2.64 ± 1.13*	2.67 ± 1.35*	0.75 ± 0.21
Serotransferrin precursor	1.0	1.11 ± 0.28	2.16 ± 0.72*	3.93 ± 0.25*	2.29 ± 0.65*	3.81 ± 1.69	0.73 ± 0.35

*Significant differences among groups for that protein (one-way ANOVA and Duncan's *post hoc* multiple comparison tests, $P < 0.05$).

Metabolic and Plasma Proteins—Within the limitations of our 2-DE analysis, we found general upregulation of glycolytic enzymes, oxidative enzymes (including mitochondrial ATP synthase), and phosphagen regulatory enzymes (creatine kinase) during unloading and early reloading (Table 3). Previous reports show similar trends in the elevation in both glycolytic and oxidative enzyme activities (*7*, *27*). As our data show relatively greater increases in glycolytic potential than in oxidative capacity (Table 3), the fast-glycolytic features of the unloaded muscle may well mask the slow-oxidative features in muscle function, such as the increase in shortening velocity. Our 2-DE analysis did not detect key glycolytic regulatory enzymes, such as hexokinase, phosphofructokinase, or pyruvate kinase. However, these enzymes were reported to be significantly upregulated in the rat soleus muscle exposed to 3 wk of hindlimb suspension (*5*), thus further confirming our observation of an overall upregulation of

the glycolytic pathway. Reduced expression of carbonic anhydrase III suggests that cellular acidosis might be enhanced due to decreased capacity of CO_2 buffering during unloading and early reloading. The significant increase in LDH expression in R2w was an unexpected result, because the trend of its expression over the unloading and reloading period was different from that of most other anaerobic enzymes (Table 3). Lactate concentration increases during unloading and decreases to the control level during reloading (*20*), and this pattern reflects changes in the proportion of fast-type fibers in the soleus muscle (*3*, *37*). Thus, this result suggests that the augmented LDH expression in R2w may effectively lower the lactate level in the tissue, while the animals might increase locomotor activities during the recovery period. Collectively, the increase in glycolytic capacity, together with upregulation of fast-type myofibrillar isoforms, would compensate for down-regulation of contractile proteins and contribute to elevation of the shortening velocity during unloading, whereas the tissue would be more susceptible to fatigue (*3*, *5*).

There need some remarks on the significant increases in the levels of three kinds of plasma proteins: hemoglobin chains, serotransferrin precursor, and serum albumin precursor. The increased levels of hemoglobin chains (oxygen transfer) and serotransferrin precursor (iron uptake and transfer) appear to support the increased aerobic potential during the unloading and reloading period. Elevation of the serum albumin precursor level suggests facilitated lipid catabolism, probably in hepatic cells, but not in myofibers where fatty acid oxidation may be limited by reduced activity of an associated mitochondrial enzyme like carnitine acyltransferase (*5*, *7*).

Lastly, it is worth noting that previous studies on muscle genes showed active transcriptional regulation of protein expression during unloading, which may further support our findings in this study. In the rodent soleus muscle, levels of α-actin mRNA, slow troponin I mRNA, and slow myosin heavy chain mRNA decreased significantly, whereas that of fast troponin I mRNA increased substantially during hindlimb unloading (*4*, *5*, *29*, *38*). The up-regulation of most transcripts in the glycolytic pathway and down-regulation of alpha crystallin B (and HSP70) (*4*, *5*, *15*) were generally in accordance with metabolic and HSP results in our study, although down-regulation of transcripts in the lipid oxidation was noticed (*5*). Thus, the outcomes of the transcriptional regulation seem to match to the corresponding protein expression in the soleus muscle, as myofibers tend to shift toward fast-phenotype during unloading. Because the muscle atrophy occurs more profoundly in slow fibers than in fast fibers, it is anticipated that transcriptional and translational activities may be reduced more severely in the former during unloading. Indeed, a significant reduction in myofibril protein contents and α-actin mRNA has been reported in the soleus muscle and, to a lesser extent, in the gastrocnemius muscle, but not in the fast-twitch extensor digitorum longus (*39*, *40*). The major loss of protein contents could be attributed to a more significant reduction in the slow myosin isoform and actin levels in the slow fibers, as well as in the HSPs (as chaperone proteins) in the unloaded muscle (*15*, *29*). Taken together, these results suggest that independent regulatory mechanisms exist in different fiber types, where unloading could affect the regulatory activities more profoundly in the slow fibers (*4*). To better understand gene regulation on changes in muscle properties under the altered loading condition, it would be important to examine transcriptional and post-transcriptional controls as well as translational modifications in a given myofiber type.

In conclusion, cellular mechanisms underlying unloading-induced muscle contractile alterations can be understood through a proteomic approach. By examining expression levels of structurally or functionally related proteins on a large scale, this biochemical approach provides us with information on what proteins are discordantly responsive to external stress. Most importantly, this approach gives us a plausible integrative interpretation of the conformational modification of the contractile apparatus and overall regulatory trends of the metabolic potential upon unloading. As HSPs are apparently crucial for maintaining and stabilizing myofibrillar integrity, it is worth investigating whether these proteins could be part of an effective countermeasure against tension reduction and atrophy during unloading of antigravity muscles (*17*).

We thank Dr. Masamichi Yamashita at the Institute of Space and Astronautical Science, Japan Aerospace Exploration Agency, Dr. E. Lee in Biomedical Proteome Research Center in Yonsei University, and an anonymous reviewer for helpful discussion and comments on this study. Dr. T. Taylor kindly assisted in editing the text. This study was supported by KOSEF R05-2003-000-10589-0 to I. Choi.

REFERENCES

1. Adams, G.R., Caiozzo, V.J., and Baldwin, K.M. (2003) Skeletal muscle unweighting: spaceflight and ground-based models. *J. Appl. Physiol.* **95**, 2185–2201
2. Baldwin, K.M. (1996) Effect of spaceflight on the functional, biochemical, and metabolic properties of skeletal muscle. *Med. Sci. Sports Exerc.* **28**, 983–987
3. Fitts, R.H., Riley, D.R., and Widrick, J.J. (2001) Functional and structural adaptations of skeletal muscle to microgravity. *J. Exp. Biol.* **204**, 3201–8
4. Cros, N., Tkatchenko, A.V., Pisani, D.F., Leclerc, L., Leger, J.J., Marini, J.F., and Dechesne, C.A. (2001) Analysis of altered gene expression in rat soleus muscle atrophied by disuse. *J. Cell. Biochem.* **83**, 508–519
5. Stein, T., Schluter, M., Galante, A., Soteropoulos, P., Tolias, P., Grindeland, R., Moran, M., Wang, T., Polansky, M., and Wade, C. (2002) Energy metabolism pathways in rat muscle under conditions of simulated microgravity. *J. Nutr. Biochem.* **13**, 471
6. Caiozzo, V.J., Haddad, F., Baker, M.J., Herrick, R.E., Prietto, N., and Baldwin, K.M. (1996) Microgravity-induced transformations of myosin isoforms and contractile properties of skeletal muscle. *J. Appl. Physiol.* **81**, 123–132
7. Fitts, R.H., Riley, D.R., and Widrick, J.J. (2000) Physiology of a microgravity environment invited review: microgravity and skeletal muscle. *J. Appl. Physiol.* **89**, 823–839
8. Ohira, Y., Jiang, B., Roy, R.R., Oganov, V., Ilyina-Kakueva, E., Marini, J.F., and Edgerton, V.R. (1992) Rat soleus muscle fiber responses to 14 days of spaceflight and hindlimb suspension. *J. Appl. Physiol.* **73**, 51S–57S
9. Riley, D.A., Bain, J.L., Thompson, J.L., Fitts, R.H., Widrick, J.J., Trappe, S.W., Trappe, T.A., and Costill, D.L. (2000) Decreased thin filament density and length in human

atrophic soleus muscle fibers after spaceflight. *J. Appl. Physiol.* **88**, 567–572
10. Isfort, R.J., Wang, F., Greis, K.D., Sun, Y., Keough, T.W., Farrar, R.P., Bodine, S.C., and Anderson, N.L. (2002) Proteomic analysis of rat soleus muscle undergoing hindlimb suspension-induced atrophy and reweighting hypertrophy. *Proteomics* **2**, 543–550
11. Yan, J.X., Harry, R.A., Wait, R., Welson, S.Y., Emery, P.W., Preedy, V.R., and Dunn, M.J. (2001) Separation and identification of rat skeletal muscle proteins using two-dimensional gel electrophoresis and mass spectrometry. *Proteomics* **1**, 424–434
12. Locke, M., Atkinson, B.G., Tanguay, R.M., and Noble, E.G. (1994) Shifts in type I fiber proportion in rat hindlimb muscle are accompanied by changes in HSP72 content. *Am. J. Physiol.* **266**, C1240–C1246
13. Neufer, P.D. and Benjamin, I.J. (1996) Differential expression of B-crystallin and Hsp27 in skeletal muscle during continuous contractile activity. Relationship to myogenic regulatory factors. *J. Biol. Chem.* **271**, 24089–24095
14. Koh, T.J. (2002) Do small heat shock proteins protect skeletal muscle from injury? *Exerc. Sport Sci. Rev.* **30**, 117–121
15. Atomi, Y., Yamada, S., Strohman, R., and Nonomura, Y. (1991) Alpha B-crystallin in skeletal muscle: purification and localization. *J. Biochem.* **110**, 812–822
16. Sugiyama, Y., Suzuki, A., Kishikawa, M., Akutsu, R., Hirose, T., Waye, M.M., Tsui, S.K., Yoshida, S., and Ohno, S. (2000) Muscle develops a specific form of small heat shock protein complex composed of MKBP/HSPB2 and HSPB3 during myogenic differentiation. *J. Biol Chem.* **275**, 1095–1104
17. Naito, H., Powers, S.K., Demirel, H.A., Sugiura, T., Dodd, S.L., and Aoki, J. (2000) Heat stress attenuates skeletal muscle atrophy in hindlimb-unweighted rats. *J. Appl. Physiol.* **88**, 359–363
18. Selsby, J.T. and Dodd, S.L. (2005) Heat treatment reduces oxidative stress and protects muscle mass during immobilization. *Am. J. Physiol. Regul. Integr. Comp. Physiol.* **289**, R134–R139
19. Isfort, R.J., Hinkle, R.T., Jones, M.B., Wang, F., Greis, K.D., Sun, Y., Keough, T.W., Anderson, N.L., and Sheldon, R.J. (2000) Proteomic analysis of the atrophying rat soleus muscle following denervation. *Electrophoresis* **21**, 2228–2234
20. Lee, K., Lee, Y.S., Lee, M., Yamashita, M. and Choi, I. (2004) Mechanics and fatigability of the rat soleus muscle during early reloading. *Yonsei Med. J.* **45**, 690–702
21. Kim, C.H., Kim do, K., Choi, S.J., Choi, K.H., Song, K.S., Chi, J., Koo, J.S., Hwang, S.Y., Yoon, J.H., and Seong, J.K. (2003) Proteomic and transcriptomic analysis of interleukin-1beta treated lung carcinoma cell line. *Proteomics* **3**, 2454–2471
22. Choi, B.K., Chitwood, D.J., and Paik, Y.K. (2003) Proteomic Changes during Disturbance of Cholesterol Metabolism by Azacoprostane Treatment in Caenorhabditis elegans. *Mol. Cell. Proteomics* **2**, 1086–1095
23. Swynghedauw, B. (1986) Developmental and functional adaptation of contractile proteins in cardiac and skeletal muscles. *Physiol. Rev.* **66**, 710–771
24. Berg, J.M., Tymoczko, J.L., and Stryer, L. (2002) *Biochemistry*, 5th ed., W.H. Freeman, New York
25. Inaguma, Y., Hasegawa, K., Kato, K., and Nishida, Y. (1996) cDNA cloning of a 20-kDa protein (p20) highly homologous to small heat shock proteins: developmental and physiological changes in rat hindlimb muscles. *Gene* **178**, 145–150
26. Srikakulam, R. and Winkelmann, D.A. (2004) Chaperone-mediated folding and assembly of myosin in striated muscle. *J. Cell Sci.* **117**, 641–652
27. Thomason, D.B. and Booth, F.W. (1990) Atrophy of the soleus muscle by hindlimb unweighting. *J. Appl. Physiol.* **68**, 1–12
28. Vandenburgh, H., Chromiak, J., Shansky, J., Del Tatto, M., and Lemaire, J. (1999) Space travel directly induces skeletal muscle atrophy. *FASEB J.* **13**, 1031–1038
29. Haddad, F., Roy, R.R., Zhong, H., Edgerton, V.R., and Baldwin, K.M. (2003) Atrophy responses to muscle inactivity. II. Molecular markers of protein deficits. *J. Appl. Physiol.* **95**, 791–802
30. St-Amand, J., Okamura, K., Matsumoto, K., Shimizu, S., and Sogawa, Y. (2001) Characterization of control and immobilized skeletal muscle: an overview from genetic engineering. *FASEB J.* **15**, 684–692
31. Littlefield, R., Almenar-Queralt, A., and Fowler, V.M. (2001) Actin dynamics at pointed ends regulates thin filament length in striated muscle. *Nat. Cell Biol.* **3**, 544–551
32. Ho, G. and Chisholm, R.L. (1997) Substitution mutations in the myosin essential light chain lead to reduced actin-activated ATPase activity despite stoichiometric binding to the heavy chain. *J. Biol. Chem.* **272**, 4522–4527
33. Cros, N., Muller, J., Bouju, S., Pietu, G., Jacquet, C., Leger, J.J., Marini, J.F., and Dechesne, C.A. (1999) Upregulation of M-creatine kinase and glyceraldehyde3-phosphate dehydrogenase: two markers of muscle disuse. *Am. J. Physiol.* **276**, R308–R316
34. Atomi, Y., Yamada, S., and Nishida, T. (1991) Early changes of alpha B-crystallin mRNA in rat skeletal muscle to mechanical tension and denervation. *Biochem. Biophys. Res. Commun.* **181**, 1323–1330
35. Gusev, N.B., Bogatcheva, N.V., and Marston, S.B. (2002) Structure and properties of small heat shock proteins (sHsp) and their interaction with cytoskeleton proteins. *Biochemistry (Mosc)* **67**, 511–519
36. Barral, J.M., Hutagalung, A.H., Brinker, A., Hartl, F.U., and Epstein, H.F. (2002) Role of the myosin assembly protein UNC-45 as a molecular chaperone for myosin. *Science* **295**, 669–671
37. Roer, R.D. and Dillaman, R.M. (1994) Decreased femoral arterial flow during simulated microgravity in the rat. *J. Appl. Physiol.* **76**, 2125–2129
38. Babij, P. and Booth, F.W. (1988) Alpha-actin and cytochrome c mRNAs in atrophied adult rat skeletal muscle. *Am. J. Physiol.* **254**, C651–C656
39. Howard, G., Steffen, J.M., and Geoghegan, T.E. (1989) Transcriptional regulation of decreased protein synthesis during skeletal muscle unloading. *J. Appl. Physiol.* **66,** 1093–1098
40. Steffen, J.M. and Musacchia, X.J. (1986) Spaceflight effects on adult rat muscle protein, nucleic acids, and amino acids. *Am. J. Physiol.* **251**, R1059–R1063